Performance of Metal Roofing to Realistic Wind Loads and Evaluation of Current Test Standards

Murray J. Morrison[1], Tim A. Reinhold[3]
[1] Insurance Institute for Business & Home Safety, Richburg, SC, USA
[2] Insurance Institute for Business & Home Safety, Richburg, SC, USA
email: mmorrison@ibhs.org, treinhold@ibhs.org

ABSTRACT: The performance of commercial roof systems to wind loads is dependent on two main factors, 1) the wind loads that the building is subjected to and 2) how these wind loads are transferred through the roof system. While there is a good understanding of the wind loads that the low-rise buildings are subjected to, the performance of the roof system is largely determined through standardized testing. These standard tests have numerous simplifications and assumption and may not be completely representative of true wind performance under real wind loading. Using the full-scale wind tunnel at the IBHS research center the external wind pressure loads on a standing seam metal roof are measured. Simultaneously the reaction loads at the clips which hold the roof panels to the roof purlins are measured directly using load cells. The current study compares the calculated reaction loads at the clips by integrating the external pressures using a geometric tributary area to the true reactions measured at each clip. It has been shown that the measured reactions at the clips from the load cell measurements are lower than those calculated from the external pressures. The lower loads are likely the result of two factors; 1) the tributary areas and structural influence functions for each clip are different that the assumed geometric tributary area. 2) For clips along the edges of the building it is likely that a significant portion of the loads on the roof are transferred to the edge. However, both the measured reactions using load cells and the integrated pressure measurements have shown a significant number of clips that exceed both the components and cladding design wind loads in the current version of the ASCE7 (ASCE-10) and also the proposed design components and cladding wind loads set to be adopted in the new version of the ASCE7 (ASCE7-16).

KEY WORDS: metal roofing; wind loads; full-scale testing; standardized testing

1   INTRODUCTION

The design and subsequent real-world performance of roof systems such as standing seam metal roofs (SSMR) for wind effects relies on two related topics: component and cladding design wind loads and standardized testing methods used to evaluate roofing systems. This paper presents results of a research program to investigate parameters which affect the conservatisms or un-conservatisms of both the design wind loads and standard test methods for low-slope commercial roof systems.

Currently, the ASCE 7 wind load subcommittee (WLSC) is evaluating a proposal to change the pressure coefficients for components and cladding (C&C) loads on flat roof buildings. The proposal reflects an increase in the state-of-the-art understanding of the wind loads on the roofs of buildings. The result is that in general, loads near the edges of the building are increasing, consistent with several studies (e.g., St. Pierre et al. [1] and Monroe [2]) who have shown that the ASCE 7 [3] pressure coefficients are in general un-conservative. Wind loads on flat roofs have relatively low spatial correlations meaning that the wind loads are reduced as the tributary areas increase (Surry et al. [4]). In practice, this is the reason pressure coefficients (GCp) in standards such as ASCE 7 [3] reduce with increasing area. As such, the application of pressures that are uniform across the entire specimen which is typical in standardized testing likely provides conservative designs. Moreover, Henderson [5] has shown that even the application of cyclical loadings, such as that found in the Australian Low-High-Low test protocol [6] for pierced metal fasteners provides conservative results when compared to the application of real wind loads.

The effect of panel size in standard tests also plays a critical role in the evaluation of the performance. For example, Schroter [7] has shown that for SSMR, the UL 580 test [8] used a specimen of insufficient size; thereby, the edge conditions overly restrain the roof specimen, reducing the overall panel deflections. Consequently, test specimens of insufficient size likely lead to un-conservative results. Currently, the effect of true edge conditions versus artificial edge conditions imposed by standard testing is not well understood. It is unclear whether true edge flashing or edge conditions provide additional hold-down as compared to standard test panels, making standard testing conservative, or if real-world edge detailing increases the loads on roof connections, making standard testing un-conservative. For example, Farquhar et al. [9] and Surry et al. [4] have shown that the ASTM E1592 test [10] is highly conservative because of the uniform loading of the panels. However, in both of their tests, no failures were observed adjacent to the edge of a building where wind load data suggests the highest loaded clips would be located. Morrison and Kopp [11] expanded on the work of Farquhar et al. [9] and showed that the lack of failure of clips along the edges would reduce the level of conservatism inherent in the ASTM E1592 test [10]. This clearly demonstrates the importance of correctly reproducing or accounting for the effects of edge conditions in the interpretation of standardized test results. Since the edge

condition used by Farquhar et al. [9] was artificial, the influence of the edge condition could not be examined. In fact, it is extremely difficult, if not impossible, to fully evaluate the effect of edge conditions without full-scale wind tunnel testing.

It is possible that the un-conservative loads provided by the current ASCE 7 C&C provisions for flat roofs combined with a conservative standard test methods yields an appropriate design solution. As the ASCE7 standard gets updated to better reflect the state-of-the-art knowledge, it makes sense to attempt to do the same with standardized test methods. The objective of the current research program is to quantify the effect of the four parameters discussed above:

1. Temporal wind fluctuations (realistic fluctuating wind pressures vs. cyclic pressures vs. static pressure)
2. Spatial uniformity of the wind load (same pressure applied everywhere)
3. Test specimen size (ASTM E1592 approximately 24 ft x 12 ft)
4. Edge condition (true edge conditions [flashing, etc.] and artificial edge conditions where the roof would continue past 12 ft and 24 ft)

Full-scale experiments in the Insurance Institute for Business & Home Safety's (IBHS) wind tunnel allow for the quantification of both the true external wind loads on an SSMR system, and the reaction loads at the clips holding the roof panels in place. The reactions at the clips are compared to calculated reactions determined by the integration of wind pressure data using a typical geometric tributary area assumption. Both the measured and computed clip reactions are also compared to both the current ASCE 7 C&C wind load provisions [3] and proposed changes to ASCE 7 C&C wind load provisions due to be included in the 2016 edition.

2   EXPERIMENT OVERVIEW

2.1   IBHS Full-Scale Wind Tunnel Building Details

A trapezoidal structural SSMR system is installed on the roof of a building with plan dimensions of 9.1 m (30 ft) x 13.7 m (45 ft), an eaves height of 3.7 m (12 ft), and a roof slope of ¼ on 12. This SSMR system is similar to the system tested by Surry et al. [4] and Farquhar et al. [9]. The metal panels had a width of 0.61 m (2 ft), with the exception of the panel in the middle of the roof which had a width of 0.3 m (1 ft) in order to achieve a full building length of 13.7 m (45 ft). The 0.3 m (1 ft) panel is installed in the center of the roof rather than at one end, which is typical construction practice, in order to maintain symmetry of the roof panels in all four corners of the roof. Figure 1 shows a photograph of the completed building inside the IBHS test chamber.

Figure 1. Photograph of the completed test building using a sculpted eave trim.

To examine the effects of different purlin spacing and corner enhancements on the load distribution through the roof, different purlin spacings are used in each corner of the roof. Figure 2 shows a schematic of the purlin layout and clip locations. On the left side of the ridge (corners #1 and #2), there are 3 purlins evenly spaced at 1.4 m (4 ft 7 in.) intervals. On the right side of the ridge (corners #3 and #4), there are 4 purlins with spacings ranging from 0.83 m (2 ft 9 in.) to 1.4 m (4 ft 6 in.). The purlins on the right side of the ridge are spaced closer together near the edge of the building and farther apart near the ridge of the roof to account for the higher wind loads that occur near the edge of the roof. In addition, a corner enhancement was installed in corners #2 and #3. This corner enhancement consists of a 1.5 m (5 ft) long purlin installed directly in the corner of the roof to provide addition clip locations (hold-downs) where the wind loads are likely to be the highest.

At each location where two panels meet and cross a purlin, a clip is attached to the purlin. The two panels are then seemed together over the clip, locking the clip into the seam. A total of 158 clips are used over the entire roof with locations shown in Figure 2. The purlin layouts on both sides of the ridge match, as closely as possible, typical purlin spacings used in practice, with corners #3 and #4 representing a design for higher wind speeds. Clearly, from the purlin spacings, it is expected that corner #1 will likely have the largest per clip loading, while corner #3 will have the lowest. The current experimental setup allowed for the changes in loads on a per clip basis to be quantified given different purling spacings. Figure 3 shows a picture of the roof purlins as the SSMR panels are being installed.

The roof system was designed and specified by the roof system manufacturer and installed by a contractor certified by the manufacturer. Once construction was completed, the manufacturer inspected the building to ensure that the SSMR was installed correctly. While insulation was not installed on the test building, the exterior of the building was sealed using typical installation practices to ensure the internal pressure inside the building would be similar to typical construction.
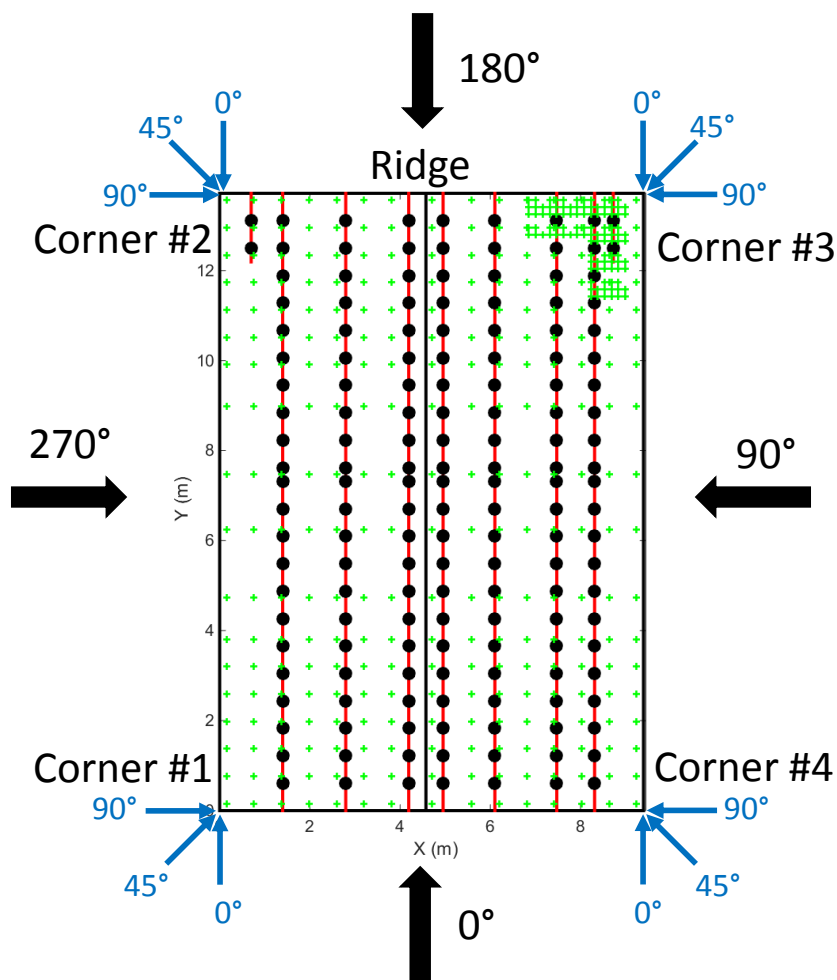

Figure 2. Plan view of the locations for purlins (red), clips (black) and pressure taps (green) on the test building. Global wind directions are shown in black while relative wind directions for each corner are shown in blue
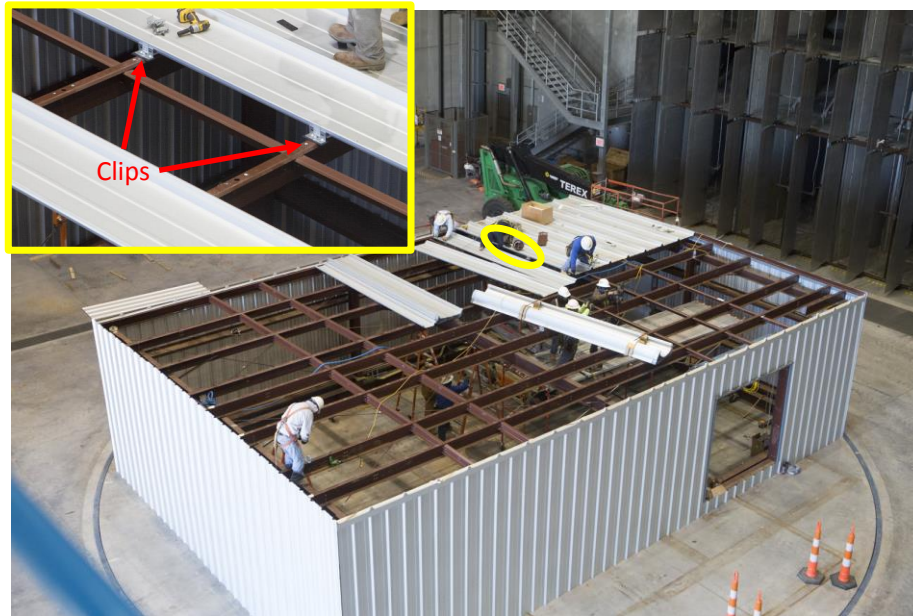
Figure 3. Photograph of the roof panels being installed. Inset shows two clips installed on the roof purlin and one panel before the second panels is installed.

2.2 Instrumentation

The external wind loads on the roof of the building were measured using 398 pressure taps as shown by the green crosses in Figure 2. As shown, there was a higher density of pressure taps in corner #3. This high-density spacing of pressure taps allowed any effect of the roof seams on the local wind pressures to be quantified. The measured pressures at each pressure tap location were referenced to the internal pressure of the building rather than a static reference pressure. By referencing the pressures to the internal pressure of the building, the pressures reflect the true wind loads on the panels themselves, and allow the pressure data to be directly compared to the loads measured by the load cell measurements described below. At 20 tap locations, duplicate pressure measurements were obtained and referenced to the typical static pressure used in the IBHS facility as discussed in Morrison et al. [12]. The internal pressure inside the building, relative to the static pressure used in the IBHS facility, was also measured independently.

The reaction loads at the clips were measured using S-beam load cells, which measure forces in a single direction. To allow for the installation of the loads cells, the installation of the clips was modified from a typical installation. Rather than the clip being screwed to the purlin, which is typical construction, a 13 mm (½ in.) hole was drilled through both the clip and the purlin. The clip was then bolted to the purling with a 6 mm (¼ in.) spacer between the clip and the purlin. This spacer ensured that the clips would be elevated above the purlin, so that when the load cells were installed and the spacer was removed, the clip would not be touching the top surface of the purlin. Figure 4 shows both a clip with and without a load cell installed. To prevent the center of the panel from floating above the purlin due to the spacer installed below the clip, a thermal spacer, as shown in Figure 4, was installed between the clips to support the center of the panel. During any test, the reactions at up to 56 clips could be measured. To measure all 158 clip locations, the load cells needed to be moved from test to test depending on which building corner was being tested. Four different load cell installations, shown in Figure 5, were used throughout testing. The locations of load cells were concentrated in the building corner being tested for each installation. Figure 6 shows the building during the roof installation prior to the installation of the ridge cap. As shown in Figure 6, the roof panels are discontinuous across the ridge of the building. Due to the flexibility of the ridge cap, it is assumed that there is little to no load transfer across the ridge. Consequently, for each load cell installation, no load cells were installed on the opposite side of the ridge from the roof corner being tested. Both the pressure and load cell measurements were sampled simultaneously at 100 Hz.
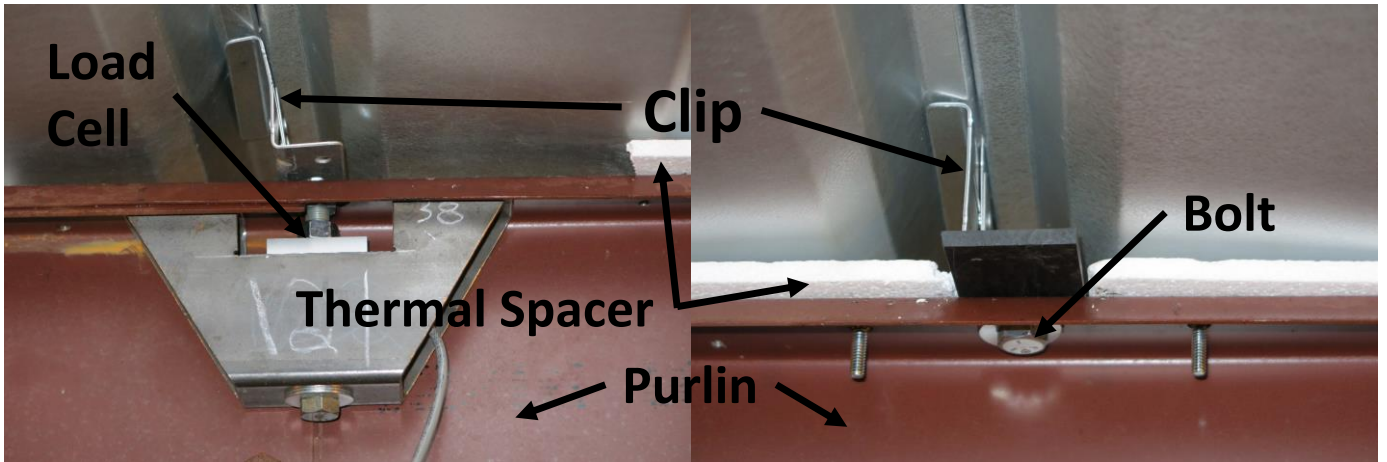
Figure 4. (Left) Clip instrumented with a load cell. (Right) clip installation without load cell.

Installation #1 (Corner #1)

Installation #2 (Corner #2)

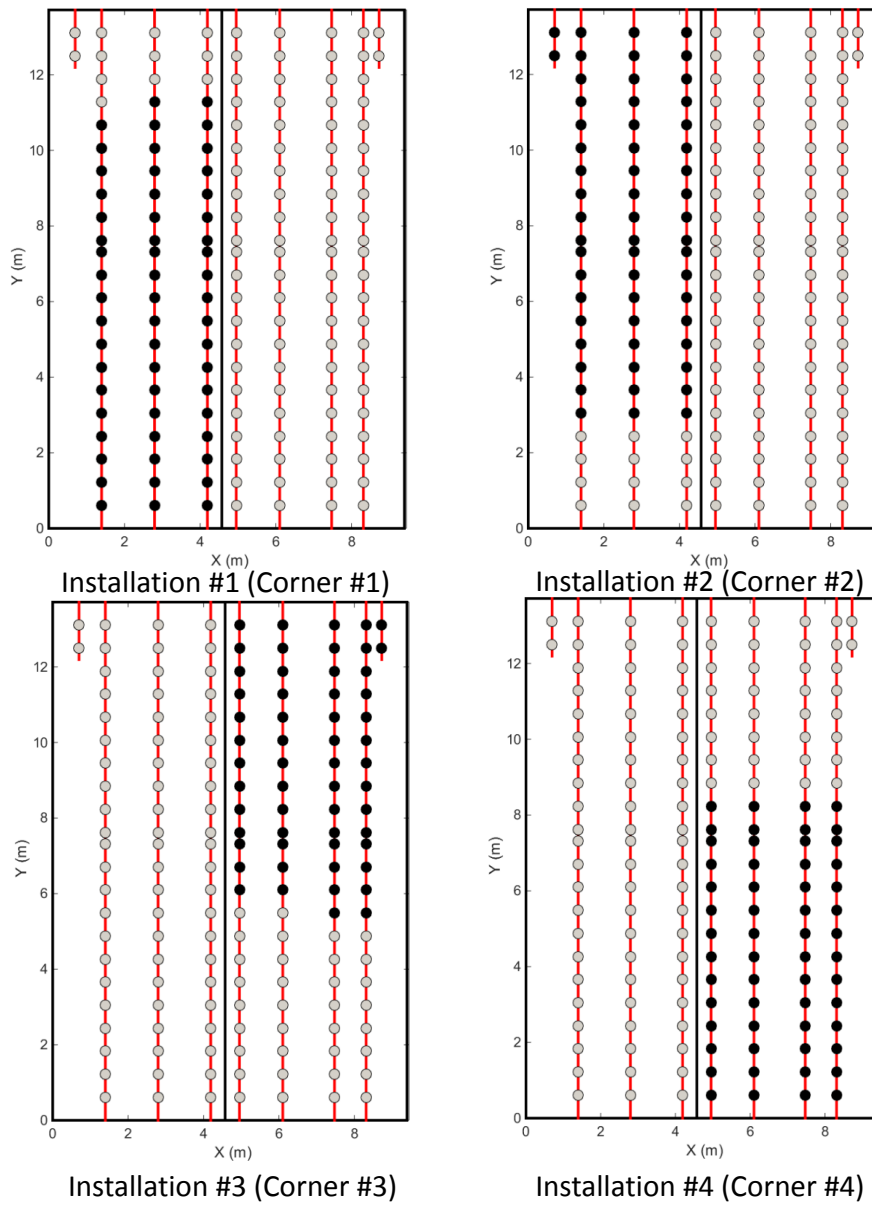Installation #3 (Corner #3)

Installation #4 (Corner #4)

Figure 5. Locations of load cells for the four different installations. Clips with load cells installed are shown in black, while clips with no load cells installed are shown in gray.
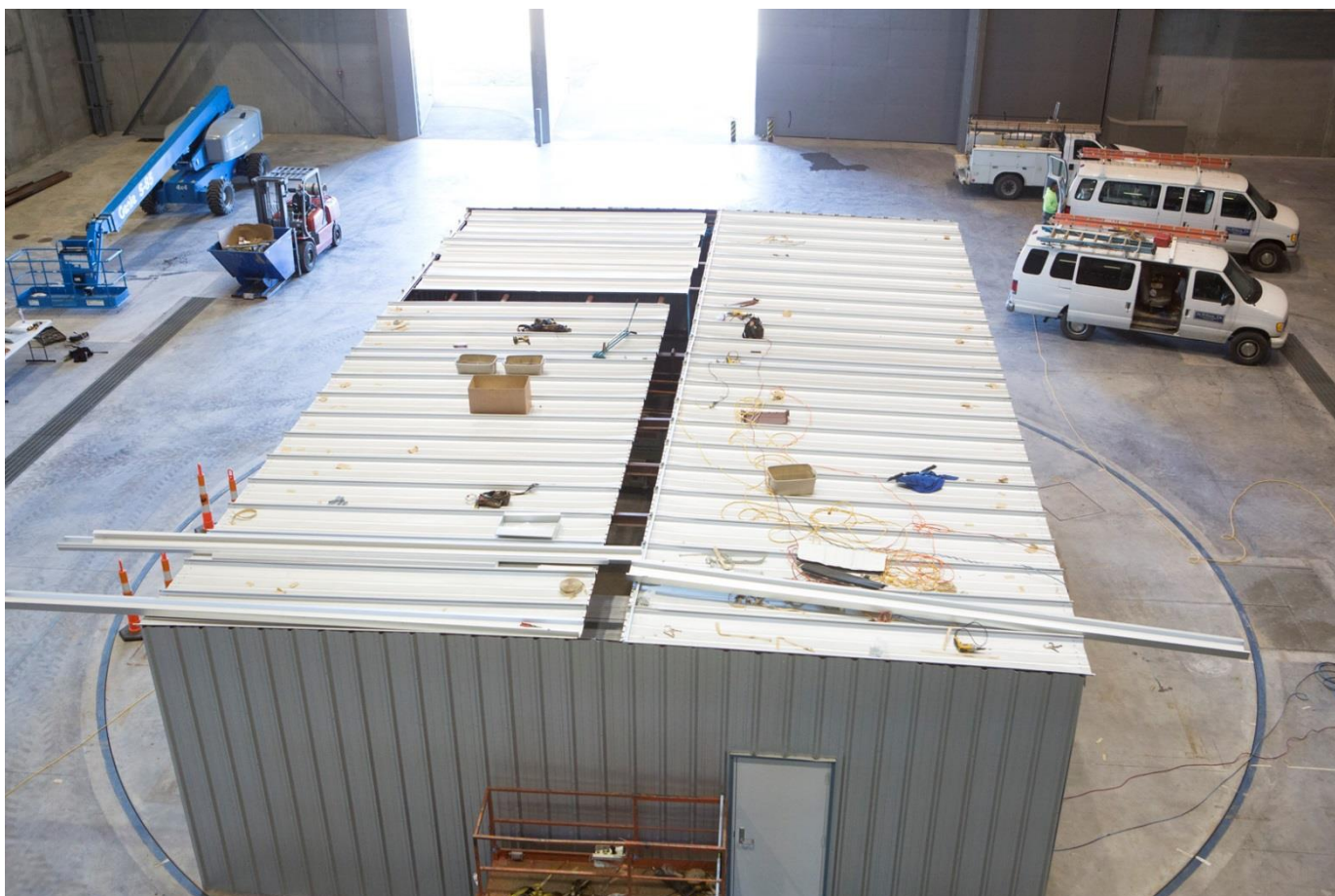
Figure 6. Roof of the test building with the panels installed on either side of the ridge prior to the installation of the floating ridge cap.

2.3 Test Protocols

For each corner of the building, tests were conducted over a 90 degree wind angle swath in 10 degree increments. To facilitate comparison of the loads from different corners, the wind angles for each corner are reported as relative wind angles for that particular corner, as shown in Figure 2, rather than the global wind angle coordinate system also shown in Figure 2.

The building is subjected to a boundary layer wind profile with an equivalent roughness length, z_o, of 0.01. Details of the flow simulation in the IBHS test chamber can be found in Morrison et al. [12]. The objective of the current experiment was to determine both the external wind pressures on the roof and the reaction loads in the clips holding the SSMR panels in place. As such, the building was tested at an initial wind speed of 25.8 m/s (58 mph)[1], at all four corners so that failure of the roof would not occur. At higher loads the panels had relatively large displacements. Therefore, once the tests at the initial wind speed were complete, higher wind speeds of 31.9, 37.2 and 44 m/s (71, 83 and 99 mph)[1] were tested at all four corners, to investigate possible changes to the load distribution due to the deflection of the panels. Tests at each wind direction and wind speed had a duration of 900 seconds.

2.4 Data Reduction

The force and pressure measurements obtained from each test are presented as non-dimensional coefficients that can be compared directly to each other and to coefficients found in ASCE 7 [3]. The measured surface pressures are normalized to a non-dimensional pressure coefficient, GCp_i using:

$$GCp_i = \frac{P_i - P_{int}}{0.5\rho V_{H,3s}^2} \tag{1}$$

where P_i is the external pressure at location i, P_{int} is the pressure inside of the building, ρ is the density of air and $V_{H,3s}^2$ is the 3-second gust wind speed at the roof height of the building.

---

[1] Wind Speeds are equivalent to design wind speeds at 10 m provided in [3]

The force measurements from the load cells are reduced into non-dimensional force coefficients, Cf_i using:

$$Cf_j = \frac{F_j}{0.5\rho V_{H,3s}^2 A_j} \tag{2}$$

where F_j is the force at clip location j, and Aj is the geometric tributary area for clip j.

Force coefficients, Cf_j^{PT}, are also calculated from the surface pressures using the same geometric tributary area, A_j, for clip j:

$$Cf_j^{PT} = \frac{\sum_{i=1}^{N}(P_i - P_{int})A_{ij} + 58.9A_j}{0.5\rho V_{H,3s}^2 A_j} \tag{3}$$

where N is the total number of pressure taps, i, on the roof of the building located within the tributary area A_j, and A_{ij} is the area of overlap between the tributary area of tap i and the tributary area of clip j. The 58.9 represents the weight of the roof panels per unit area in Pa.

3   RESULTS

3.1   Building Internal Pressures

Figure 7 shows the mean GCp pressures across the roof panels for wind angles normal to the four walls (i.e., 0, 90, 270 and 360 degrees) as indicated in Figure 2. As shown in Figure 7b, the wind pressures at a wind angle of 90 degrees have significantly higher uplift pressures on the roof of the building than any of the other wind directions. It would have been expected that the magnitudes of the uplift pressures at each of the wind angles presented in Figure 7 would have been similar given that all wind angles are normal to one of the walls. Figure 8 shows results for the same wind directions as Figure 7 except that the pressures have been shifted by the corresponding mean internal pressures at each wind angle. Figure 8 clearly shows that the difference in the magnitudes of the pressures on the roof panels shown in Figure 7 can be attributed to different internal pressures inside the building at each corresponding wind angle. Figure 9 presents the variation of maximum, minimum and mean internal pressures inside the building as a function of wind angle. The inset in Figure 9 shows the locations of the roll-up door and personnel doors (which can been seen in Figure 1 and Figure 3) relative to the wind direction. Clearly there is a strong dependence of internal pressure relative to the orientation of the roll-up door to the oncoming wind direction. At wind angles between 30 and 160 degrees where positive external pressures would be expected at the location of the roll-up door, the internal pressures are positive, with the highest internal pressures occurring at wind angles between 90–110 degrees. In contrast, the largest suction pressures (negative pressure) at the location of the roller door would be expected at a wind angle of approximately 0 degrees.

The wind angle which produces the worst net wind pressures on the roof of the building may not correspond to the wind angles presented in Figure 7. In fact, differences in internal pressure when the worst net external pressures occur for each load cell installation may be less than what Figure 7 suggests. Figure 10 presents the largest negative mean net pressures over all relative wind angles of 0 to 90 degrees (shown in Figure 2) for each corner. Figure 10 clearly shows that at the wind direction where the worst mean net pressures occur, there is still a substantial difference between each corner, although the differences between each corner are less than the differences shown in Figure 7. Interestingly, it appears that the worst net mean pressures are similar for

corners #1 and #2, and for corners #3 and #4, suggesting that it may be possible to compare results for these two groups of corner clips directly.
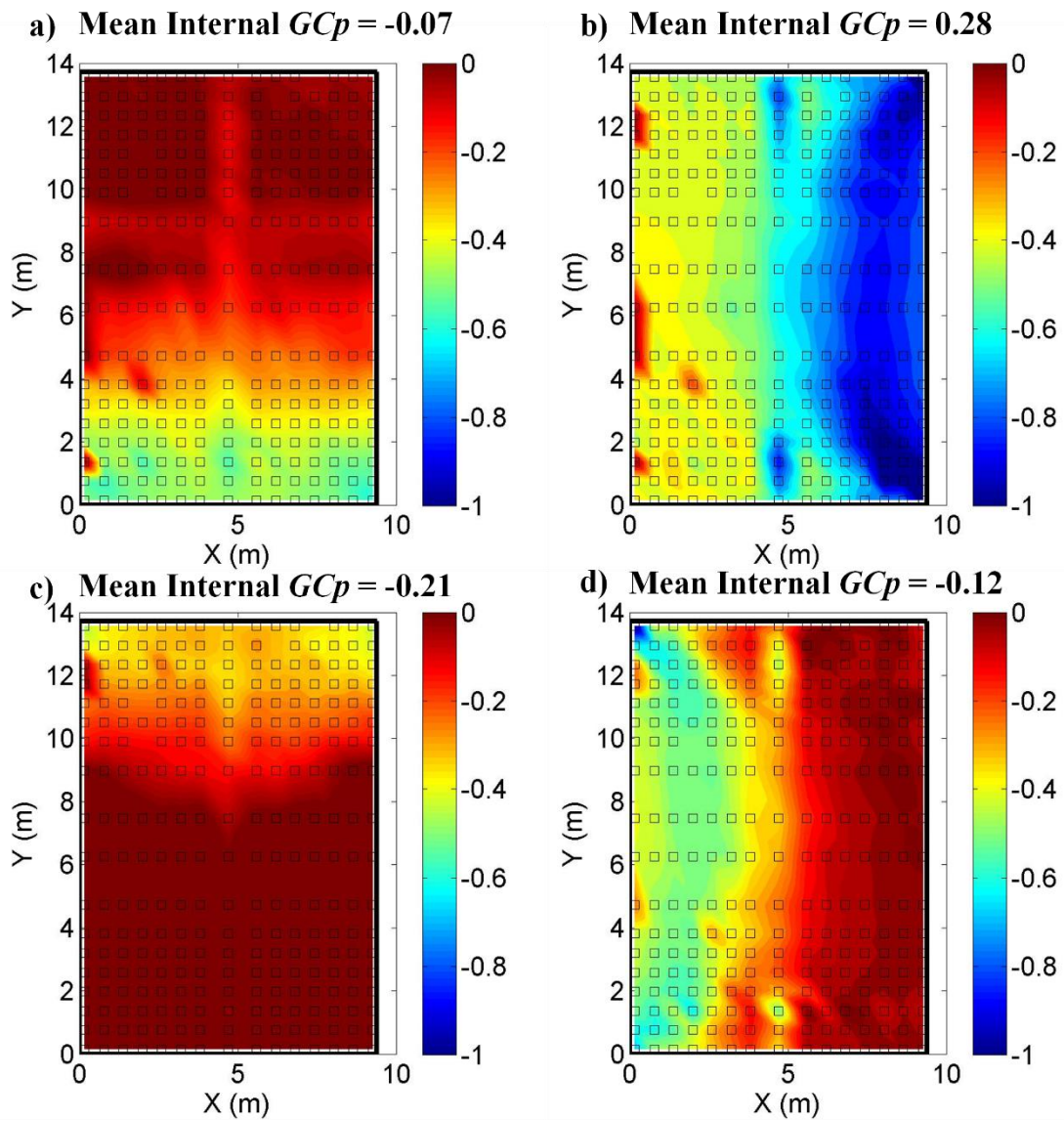
a) Mean Internal *GCp* = -0.07

b) Mean Internal *GCp* = 0.28

c) Mean Internal *GCp* = -0.21

d) Mean Internal *GCp* = -0.12

Figure 7. Contours of net negative (uplift) pressures across panels (a) 0 degrees, (b) 90 degrees, (c) 180 degrees, and (d) 270 degrees.
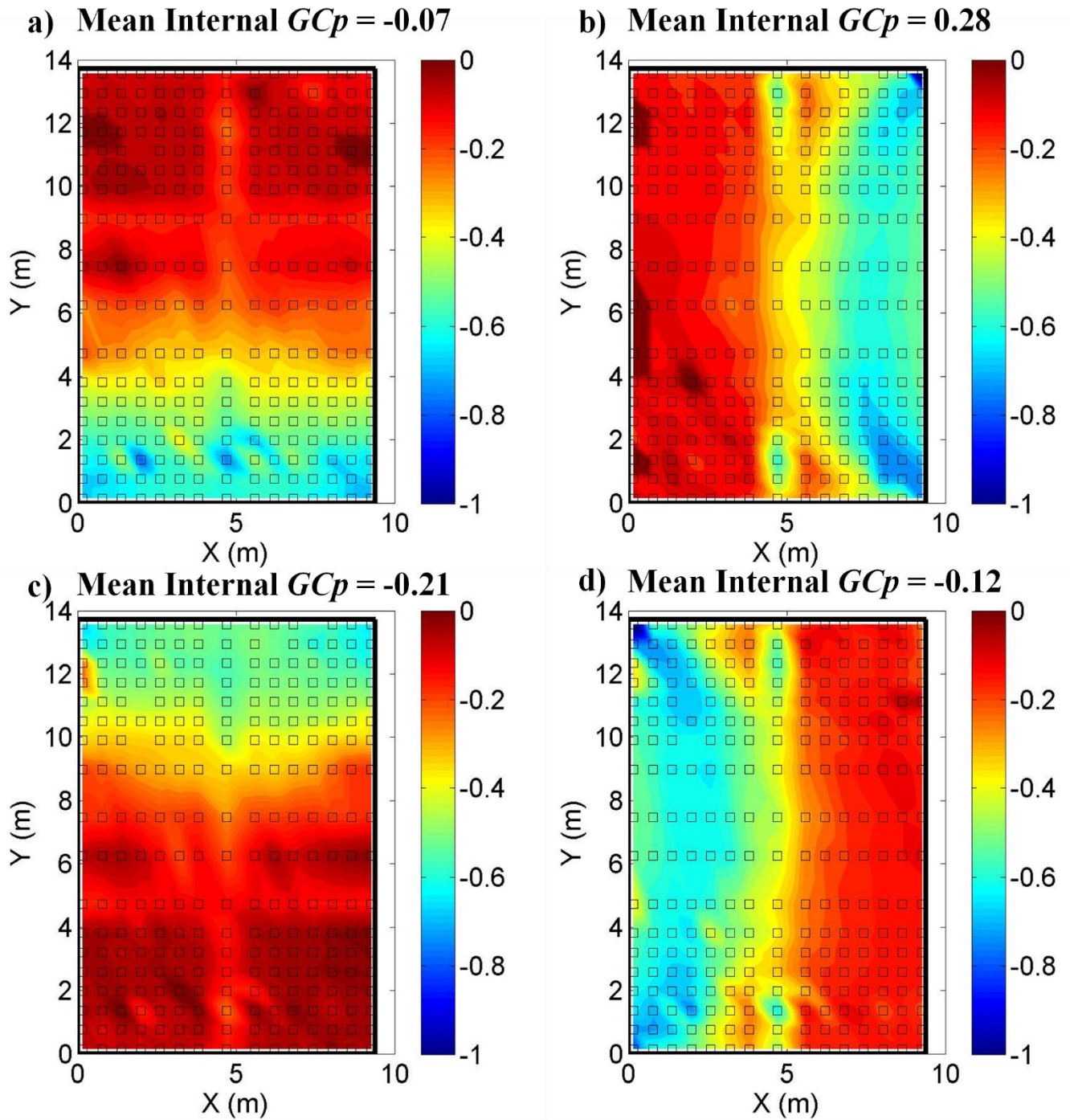
a) Mean Internal *GCp* = -0.07

b) Mean Internal *GCp* = 0.28

c) Mean Internal *GCp* = -0.21

d) Mean Internal *GCp* = -0.12

Figure 8. Contours of net negative (uplift) pressures across panels, shifted by the mean internal pressure measured inside the building: (a) 0 degrees, (b) 90 degrees, (c) 180 degrees, and (d) 270 degrees.
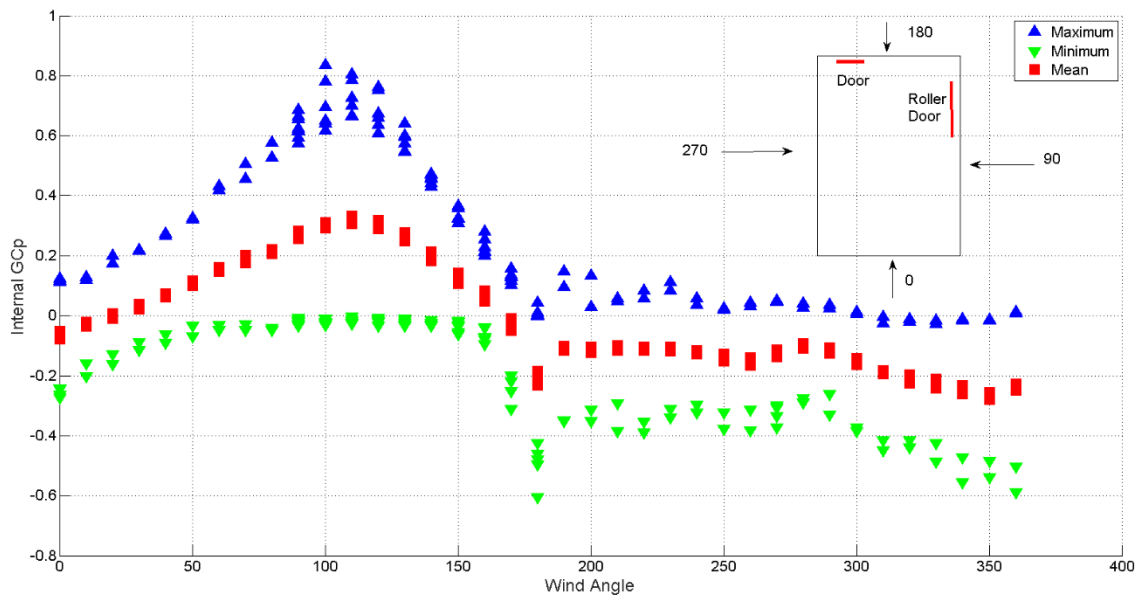
Figure 9. Variation of internal pressure with wind angle.

The implications of the roll-up door appearing to act as a dominant opening to the building is that while the external wind pressures are the same for each corner, the net wind load on the roof panels at each corner are different. As a result, the load cell results from all four corners and net pressures across the roof panels cannot be compared directly. A correction for the internal pressure is required to compare net pressures across the roof deck from one corner to another. While the internal pressures inside the building vary in time, they act uniformly over all of the roof panels, meaning the spatial variation of the pressures acting on the panels will be similar in each corner at the same relative wind angles, defined in Figure 2. Moreover, since the pressure transducers in the current experiment measure the difference in pressure between the external pressure and the internal pressure of the building, the true net wind loads, regardless of internal pressure, are measured. As such, the wind loads measured by the load cells at each clip can be compared directly to the measured wind pressures. However, due to the low and variable spatio-temporal correlation between the internal pressures at various wind directions and the roof pressures, direct comparison between the measured wind load coefficients obtained in the current study with the coefficients provided by ASCE 7 [3] is challenging.
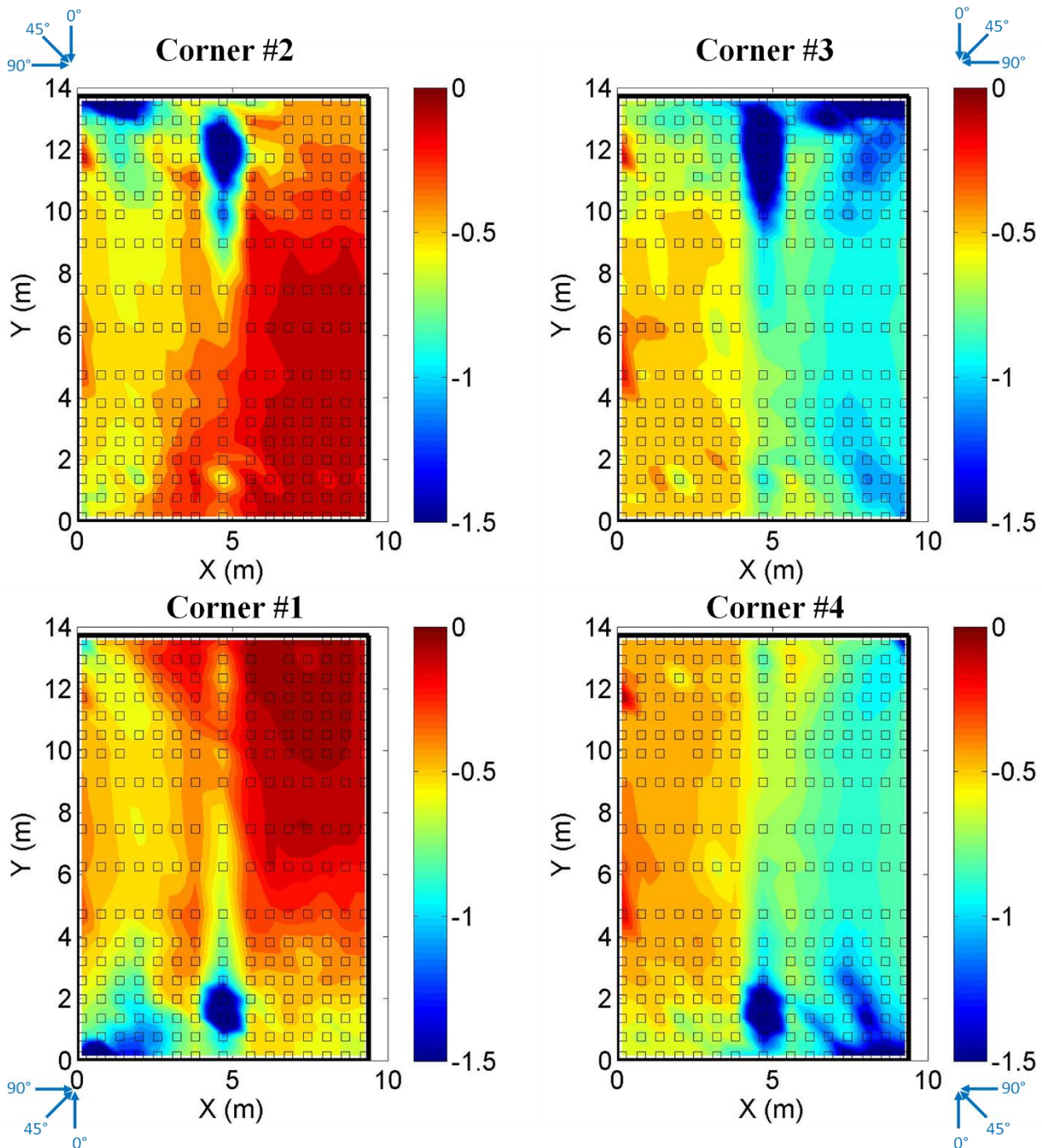
Figure 10. Contours of the peak mean net pressures over all wind angles tested for each corner when the loads cells are installed in that corner (i.e., relative wind angles of 0 to 90 degrees presented in Figure 2).

3.2 Clip Loads

Figure 11 through Figure 14 present the worst peak uplift force coefficients from both the load cells (Cf) and pressure measurements (Cf^{PT}) for corners #1, #2, #3 and #4 respectively over all relative wind angles tested for each corner. The black dots in Figure 11 through Figure 14 represent the instrumented clips for each corner. Pressure-based uplift force coefficients are shown as constant over the tributary area for each clip. In general there is fairly good agreement between the force coefficients based on load cell measurements and those based on the integrated pressure data. However, in an overall sense, the integrated pressure data appear to overestimate the loads at the clips. In particular, the integrated pressure analysis suggests clip uplift loads should generally be higher near the edge of the roof and the higher uplift loads should extend farther into the field of the roof than shown by the load cell measurements. One possible reason for the higher loads from the integrated pressure data is the deflection of the roof panels that occurs under high wind loads. As an example, Figure 15 shows a photograph of the roof panels both before testing when no wind is blowing on the building, and during a test when the building is subjected to high wind loads. As indicated in

Figure 15, the pans have deflected significantly from their unloaded state. Since the roof pressures act normal to the surface of the panels, the deflection of the panels results in lateral reactions at the clips which would not be measured by the single-axis load cells used in the current experiment. Furthermore, the deflection of the panels into a near quarter-circle cross section extending along the length of the panel, may help the panels act more like a beam, resulting in a redistribution of forces along the length of the panel and into the edge flashing. Moreover, the difference between the load cell and integrated pressure measurements are most significant at clip locations that are adjacent to the edge of the building, indicating that a significant portion of the loads are being resisted at the edge condition of the building. As hypothesized in the previous section, the loads in corners #1 and #2 are similar and are lower in magnitude than those from corners #3 and #4.
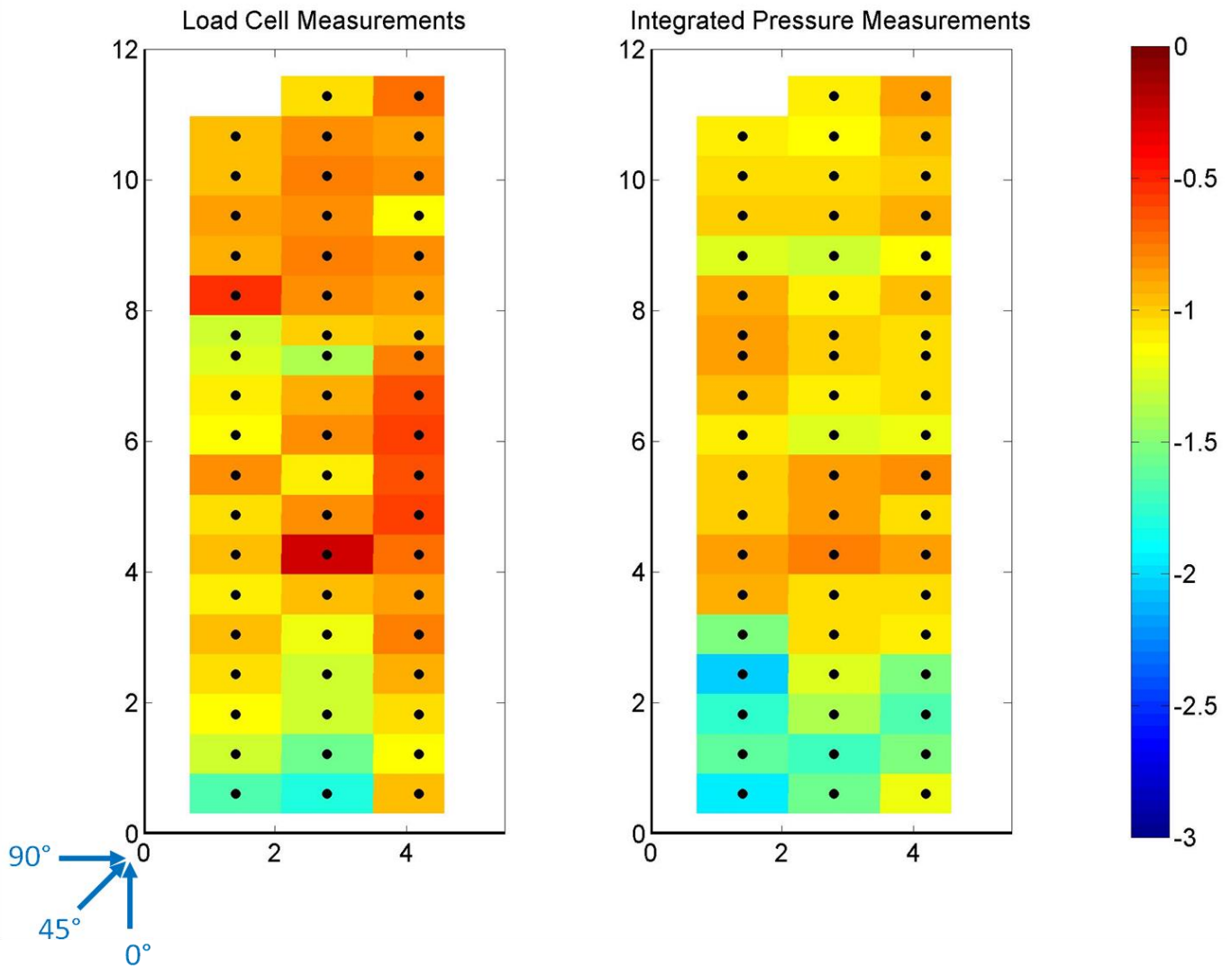

Figure 11. Contours of the peak load coefficient, *Cf* at each clip in installation #1 (corner #1). (Left) From the load cell measurements. (Right) From integration of the net surface pressures.
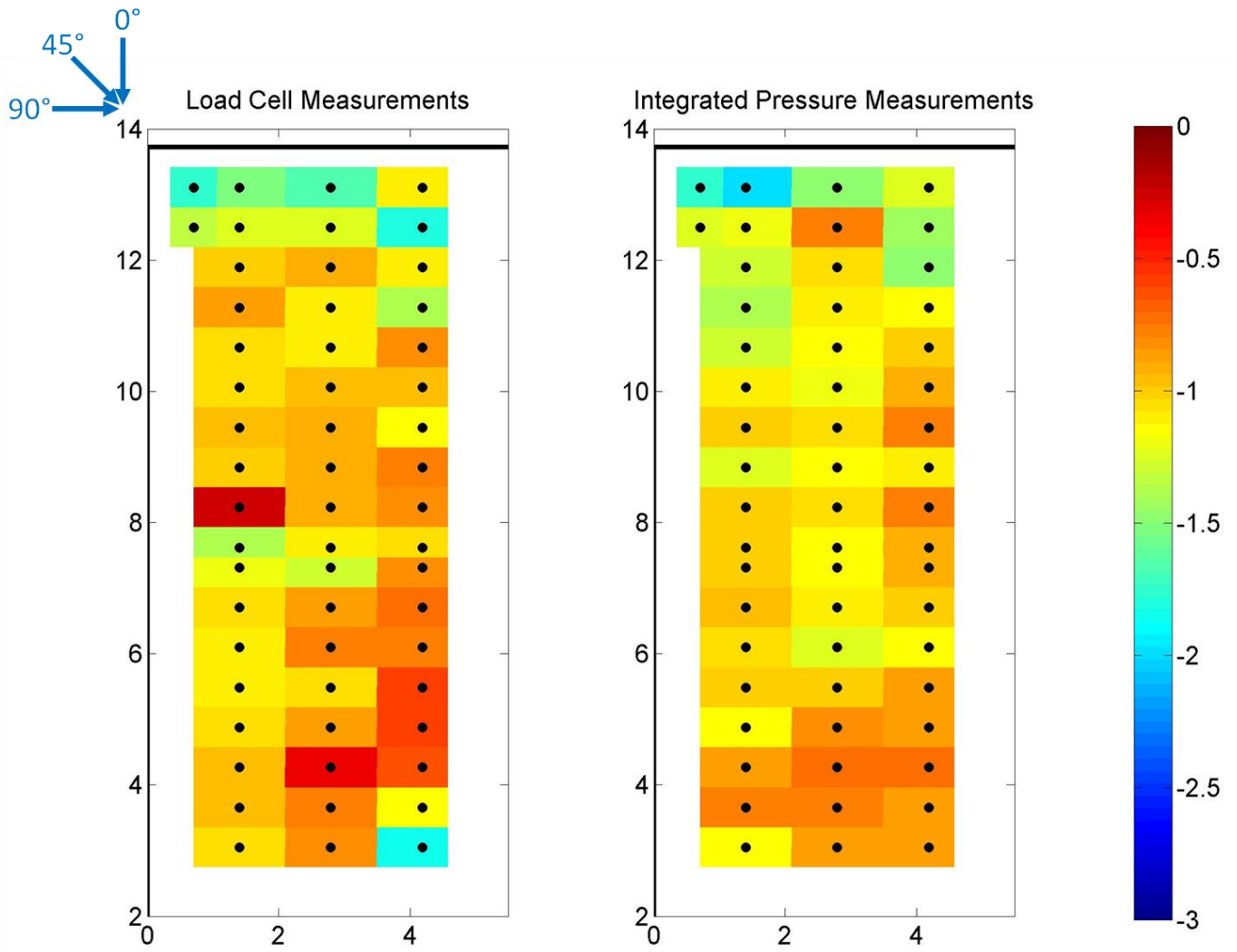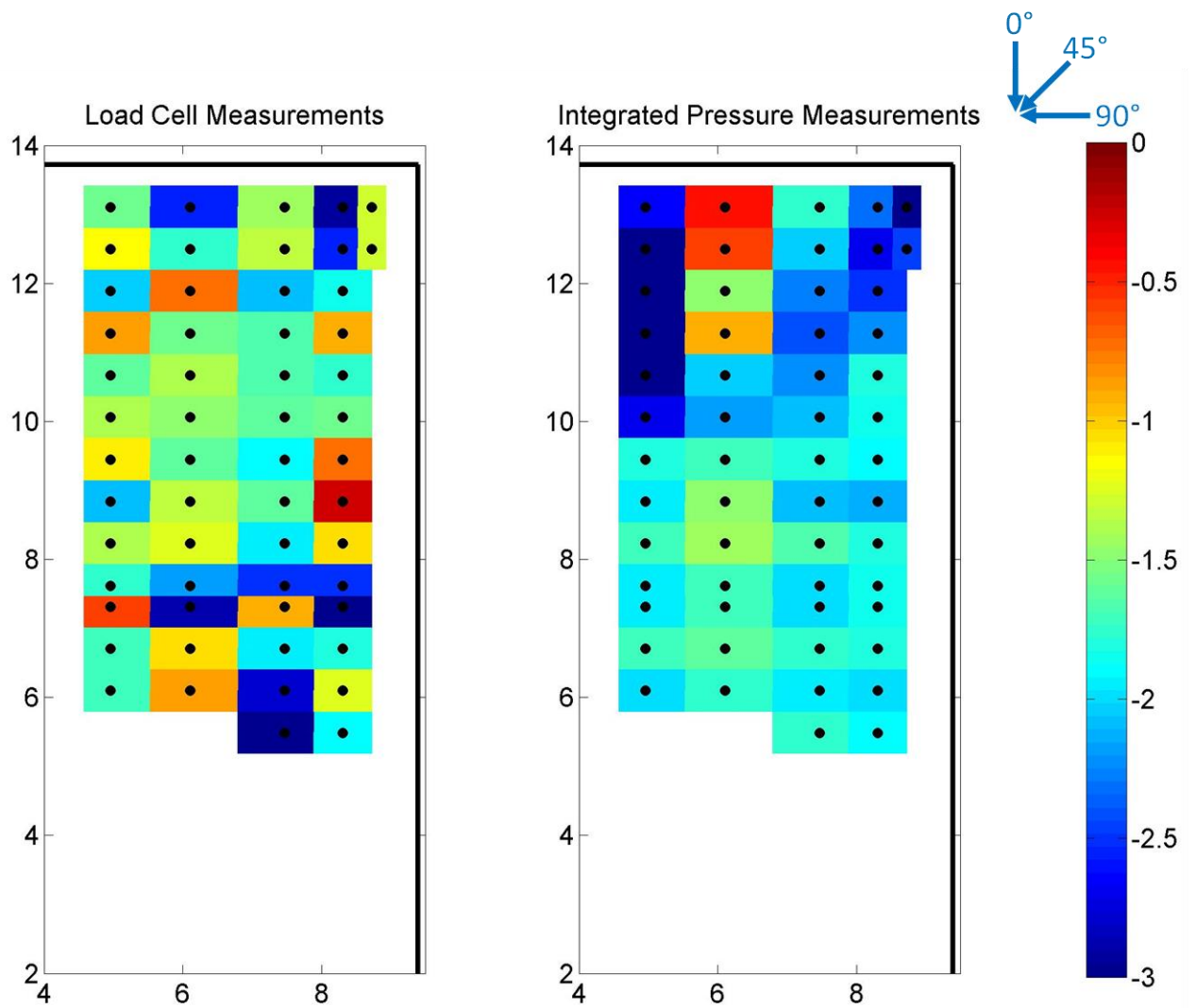
Figure 12. Contours of the peak load coefficient, *Cf* at each clip in installation #2 (corner #2). (Left) From the load cell measurements. (Right) From integration of the net surface pressures.

Figure 13. Contours of the peak load coefficient, *Cf* at each clip in installation #3 (corner #3). (Left) From the load cell measurements. (Right) From integration of the net surface pressures.
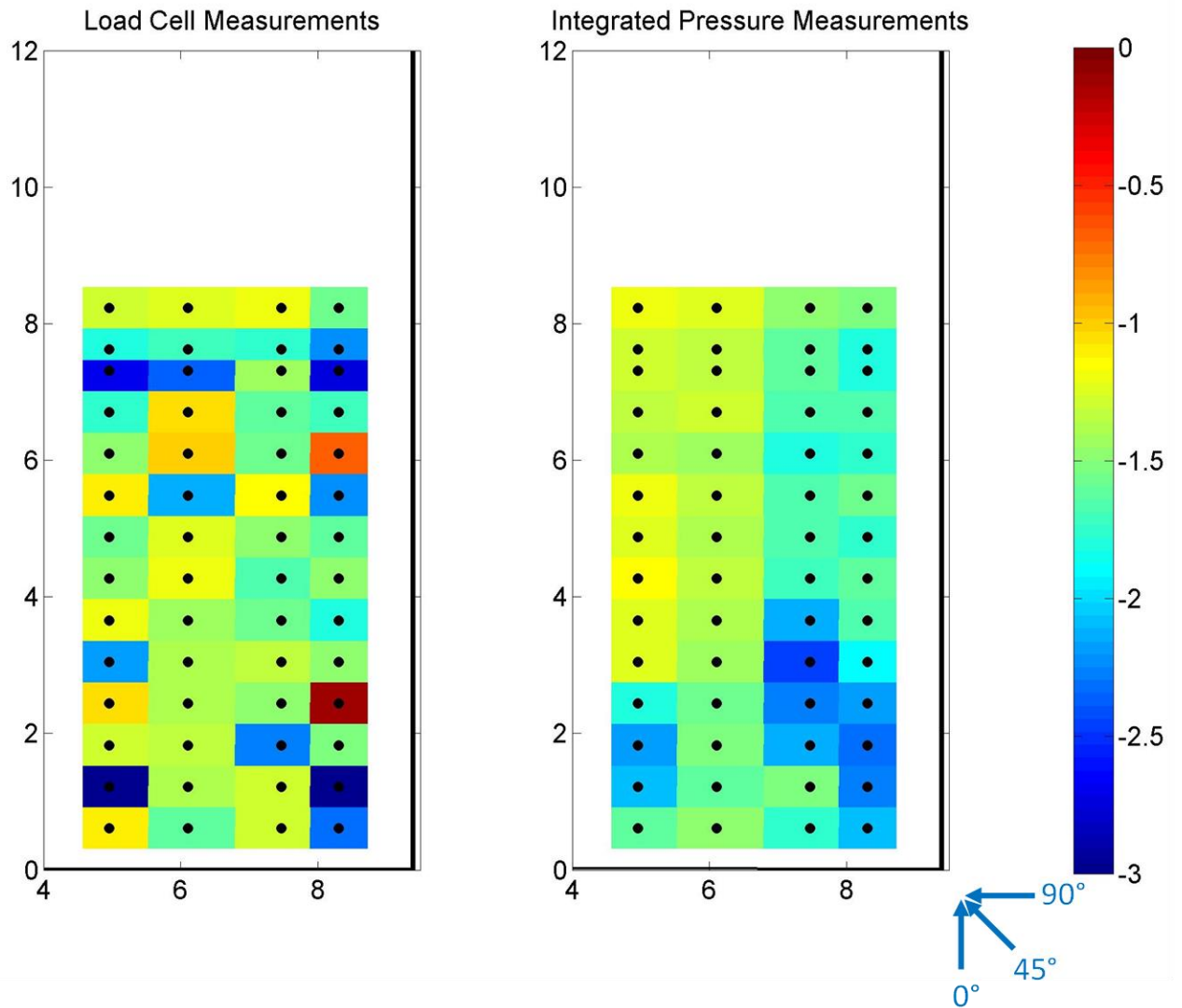
Figure 14. Contours of the peak load coefficient, *Cf* at each clip in installation #4 (corner #4). (Left) From the load cell measurements. (Right) From integration of the net surface pressures.
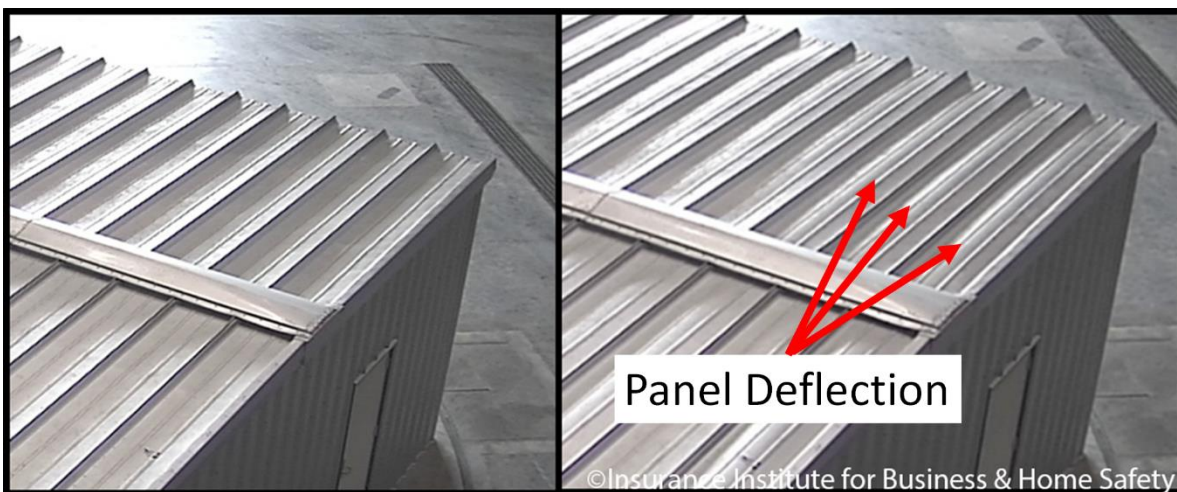

Figure 15. (Left) Photograph of the roof panels under no wind load. (Right) Photograph of the deflection of several panels under high wind loads.

3.3   Comparison of Measured Clip Loads Compared to ASCE7-10 Design Loads

As discussed in section 3.1, a direct comparison of the measured force coefficients to ASCE 7 [3] is challenging due to the internal pressure inside the building. However, over the wind angles at which corner #2 was tested, from 180 to 270 degrees, the mean internal pressure was nearly constant with a value of approximately -0.21. Due to the negative pressure inside the building for all wind angles tested when corner #2 was instrumented, the resultant forces on the clips should be lower than the external C&C design pressures provided by ASCE 7 [3]. Figure 16 presents the percent difference between the measured clip uplift force coefficients (from both the load cells and integrated pressure measurements) and the clip uplift force coefficients calculated using ASCE 7 [3]. The percent difference is determined by:

$$Percent\ Difference = \left[\frac{Cf_j^{PT} or\ Cf_j}{Cf_j^{ASCE7-10}} - 1 \right] * 100 \qquad (4)$$

where $Cf_j^{ASCE7-10}$ is the uplift force coefficient calculated for each clip from ASCE 7 [3].

Using Eq. 4, percent differences that are positive mean that the measured clip uplift coefficients exceed those calculated using ASCE 7, or in other words, the ASCE7-10 standard [3] is not conservative. Negative percent difference values mean that the ASCE7-10 standard [3] is conservative relative to the measured clip uplift force coefficients.

In Figure 166, the percent difference for each clip location is shown using one of six different color groups as described in Table 1. Figure 166 shows that nearly half the clips in this corner have uplift force coefficients that exceed those calculated from ASCE 7 [3]. In most cases, the exceedance is less than 10%; however, certain clips have exceedances greater than 40%. Moreover, all of the clips where the percent difference is greater than 0 are in the interior zone of the roof as defined by ASCE 7 [3]. This is consistent with findings from Morrison and Kopp [11] which showed that clips in the interior zone adjacent to the edge and corner zones had wind loads that were underestimated by ASCE 7 [3].
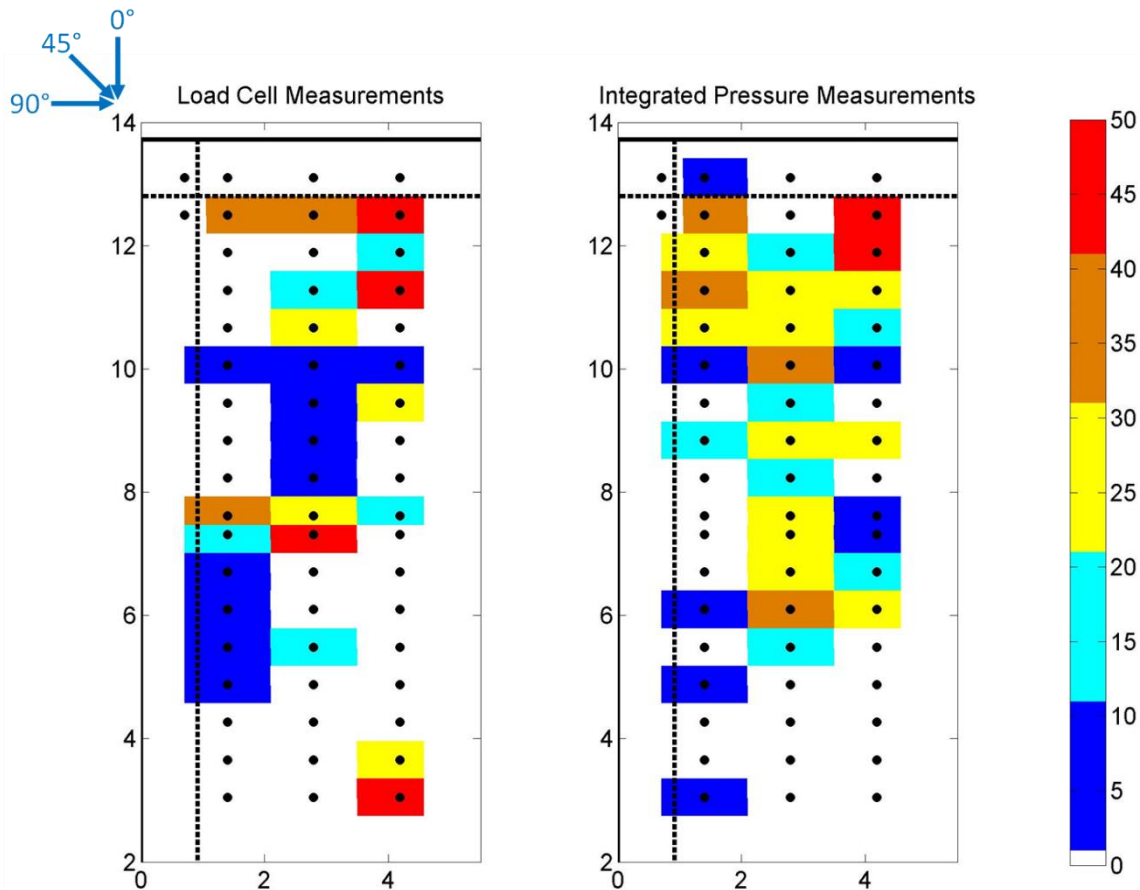

Figure 16. Contours of the percentage difference between the peak load coefficient, *Cf* and the calculated load coefficients from the components and cladding loads found in the ASCE7-10 [3] for installation #2 (corner #2). (Left) Load cell measurements. (Right) Integration of the net surface pressures using a geometric tributary are for each load cell location. The black lines in each plot represent the ASCE 7 roof zones for the test building.

Table 1. Colors used for different ranges of percent difference in Figures 16.

Figure 16	
Percent Difference (%)	Color
<0 %	White
0 to 10%	Blue
10 to 20%	Teal
20 to 30%	Yellow
30 to 40%	Brown
>40%	Red

Figure 17 and Figure 18present the percent difference using both the current version of the ASCE7 code and the proposed changes for of all clips in each of the four corners of the building (not measured simultaneously) for both the load cell and integrated pressure measurements, respectively. The results in both Figure 17 and Figure 18 are sorted from highest percent difference to lowest. Because certain clips were measured in multiple load cell installations, the total number of clips shown in Figure 17 and Figure 18 is 224 rather than 158 which is the total number of clips on the building. When comparing to the current version of the ASCE7-10, there are a significant number of clips with positive percent differences when using both the load cell measurements and the loads from the integrated pressure measurements. In fact, for the load cell measurements, 146 of the 224 clips (65% of the clips) had positive percent differences while 210 (94% of the clips) had positive percent difference when using the integrated pressure measurements. When comparing to the proposed C&C loads for the ASCE7-16, significantly fewer clip locations had positive percent differences: 29 (13%) for the load cell measurements and 62 (28%) for the integrated pressure measurements. The current results indicate that the proposed changes to the C&C loads better envelope the loads on SSMR clips for the current building configuration than the current version of the ASCE7 standard.
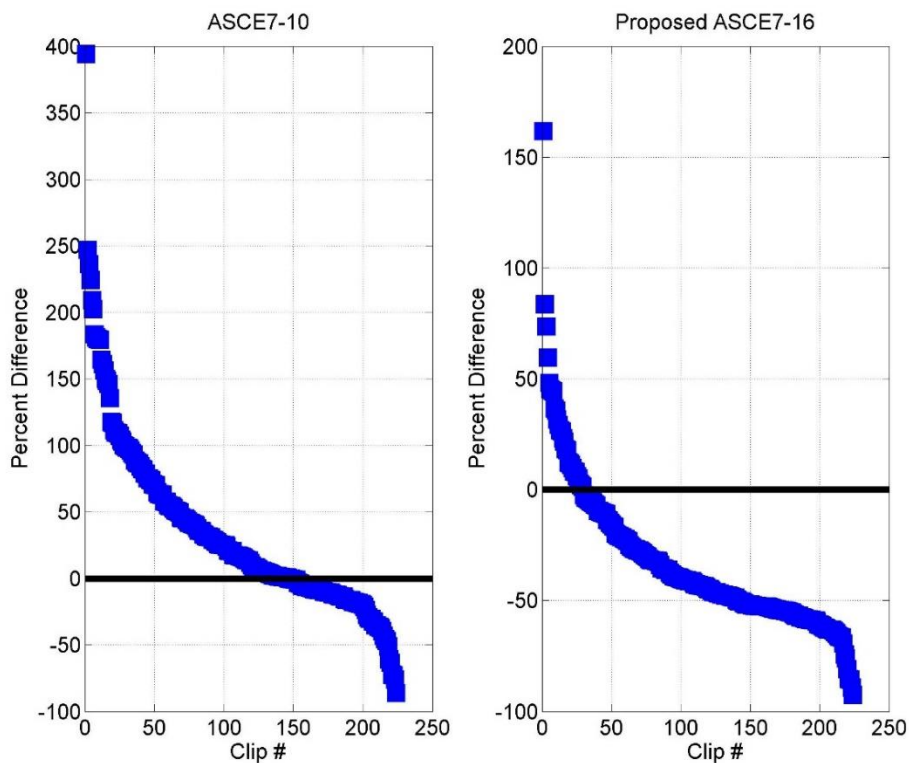

Figure 17. Percent difference for all clips measured in all four corners (not simultaneously) using the load cell measurements for both the current version of the ASCE7 [3] (Left) and for the proposed version of the ASCE 7 (Right).
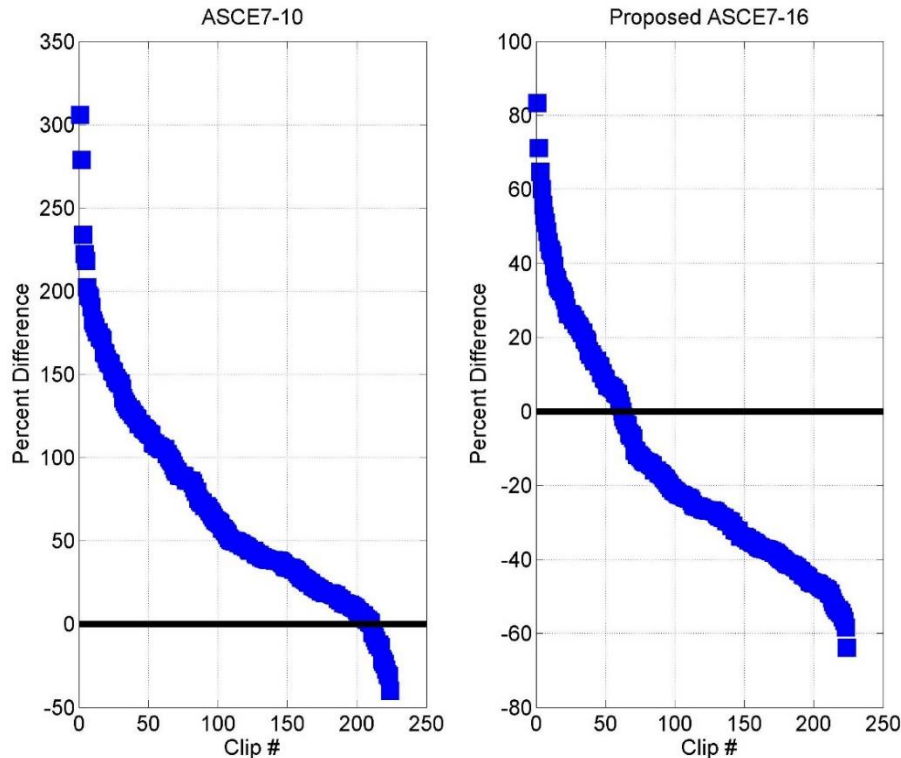
Figure 18. Percent difference for all clips measured in all four corners (not simultaneously) using the integrated pressure measurements for both the current version of the ASCE7 [3] (Left) and for the proposed version of the ASCE 7 (Right).

4   CONCLUSIONS

The current paper presented measurements of both the net pressure loads across a standing seam metal roof and the reaction loads at the clips used to hold the roof panels to the purlins. Generally, good agreement has been found between the reactions at the clips measured by single-axis load cells and integrated pressure measurements using a tributary area assumption. The loads on the clips have found to exceed those calculated using the current version of the ASCE7-10 [3] even when a high negative internal pressure was present. In contrast, the proposed changes to the ASCE7 C&C external wind loads for the 2016 version of the ASCE7 appear to be conservative, but not overly so, for the current building configuration.

REFERENCES

[1]   L. St. Pierre, G. A. Kopp, D. Surry, *The UWO contribution to the NIST aerodynamic database for wind loads on low buildings. II. Comparison of data with wind load provisions,* Journal of Wind Engineering and Industrial Aerodynamics, 93, 31-59, 2005.
[2]   J.S., Monroe, *Wind Tunnel Modeling of Low Rise Structures in a Validated Open Country Simulation,* MS Thesis, Department of Civil Engineering, Clemson University, Clemson, SC, 1996.
[3]   American Society of Civil Engineers (ASCE), *Minimum Design Loads for Buildings and Other Structures,* American Society of Civil Engineers Structural Engineering Institute, Reston, VA, 2010.
[4]   D. Surry, R.R. Sinno, B. Nail, T.C.E. Ho, S. Farquhar, G.A. Kopp, *Structurally Effective Static Wind Loads for Roof Panels,* Journal of Structural Engineering, 133(6), 871-885, 2007.
[5]   D.J. Henderson, *Response of pierced fixed metal roof cladding to fluctuating wind loads,* PhD thesis, School of Engineering and Physical Sciences, James Cook University, Townsville, Queensland, Australia, 2010.
[6]   BCA., *Building Code of Australia,* A.B.C. Board, ed., ABCB, Canberra, 2006.
[7]   R.C. Schroter, *Air pressure testing of sheet metal roofing, a decade of change and future trends in roofing,* Proceedings of International Symposium on Roofing Technology. National Roofing Contractors Association, Gaithersburg, MD, 1985.
[8]   Underwriters Laboratories (UL 580), *Test for Uplift Resistance of Roof Assemblies*, Standard UL 580. Northbrook, Ill, 1996.
[9]   S. Farquhar, G.A. Kopp, D. Surry, *Wind tunnel and uniform pressure tests of a standing seam metal roof model,* Journal of Structural Engineering, 131(4), 650–659, 2005.
[10]   American Standard for Testing and Materials (ASTM), *Standard test method for structural performance of sheet metal roof and siding systems by uniform static air pressure difference*, E 1592-01, ASTM International, West Conshohocken, Pa, 2001.
[11]   M.J. Morrison, G.A, Kopp, *Analysis of Wind-Induced Clip Loads on Standing Seam Metal Roofs*, Journal of Structural Engineering, 135(3), 334-337, 2010.
[12]   M.J. Morrison, T.M. Brown, Z. Liu, *Comparison of field and full-scale laboratory peak pressures at the IBHS Research Center,* In: Proceedings of the ATC-SEI Advances ibn Hurricane Engineering Conference, Miami, FL., 2012.
[13]   G.A. Kopp, M.J. Morrison, D.J. Henderson, *Full-scale testing of low-rise, residential buildings with realistic wind loads,* Journal of Wind Engineering and Industrial Aerodynamics, 104-106, 25-39, 2012.